Authors' accepted manuscript.
Article published in *IEEE Transactions on Ultrasonics, Ferroelectrics, and Frequency Control* (Volume: 69, Issue: 4, April 2022)
Version of record available at: https://doi.org/10.1109/TUFFC.2022.3148676

A Nonlinear Pulse Shaping Method Using Resonant Piezoelectric MEMS devices

Mathieu Gratuze, *Student Member, IEEE*, Abdul-Hafiz Alameh, *Member, IEEE*, Alexandre Robichaud, *Member, IEEE*, and Frederic Nabki, *Member, IEEE*

***Abstract*—In this paper, a methodology for increasing the displacement of the membrane in nonlinear transducers is presented. This methodology that relies on pulse shaping is based on the frequency modulation of the excitation signal which in turn results in an amplitude modulation of the displacement of the resonator. The benefits of pulse shaping include the increase of the displacement of the membrane of the resonator, the ability to leverage two mechanisms to dynamically tune the resonant frequency of the device and a relative control of the decay time of the resonator. These properties have been verified using simulations and experimental results. The experimental results are performed using two nonlinear resonators with a frequency of 3.9 kHz and 7.9 kHz. With a constant amplitude of the excitation voltage, experimental results show that the use of pulse shaping allows a velocity increase of the membrane of a piezoelectric MEMS resonator of up to 191% for a softening type resonator, and 348% for a hardening type resonator. The frequency tuning mechanism allowed the operation of the softening type resonator and of the hardening type resonator over a bandwidth of 280 Hz and 115 Hz, respectively, while providing higher velocity than with the non-optimized excitation signal. The resulting pulse shaping methodology can be applied to other nonlinear resonators as shown using simulation and experimental results. Therefore, this work should lead to an increase of the use of nonlinear resonators for various applications.**

***Index Terms*—Nonlinearity, Piezo-eletricity, Pulse Shaping, PMUT, Transducer, Duffing resonator, Softening, Hardening, Frequency Tuning**

I. Introduction

PIEZOELECTRIC Micromachined Ultrasonic Transducers (PMUTs) are a major innovation in ultrasound technology [1–3], as these devices offer better performance in terms of bandwidth, resolution and penetration than traditional ultrasonic transducers at very low cost. These devices allow for the creation and reception of acoustic signals using micro-electromechanical systems (MEMS). The operation frequency of these devices ranges from a few kHz to a few MHz [4], [5]. Applications for these devices include imaging in both medical and non-medical applications, in addition to ranging and non-destructive testing [6–10]. In these applications, PMUTs offer better performance, in terms of bandwidth, and resolution, than the piezoceramics used in current solutions. It should be noted that PMUTs are part of a larger family of micromachined ultrasonic transducers (MUTs), and that new applications are enabled thanks to their properties. For example, it has been shown that PMUTs can act as an active terahertz time differentiator [11–13], in which case the periodic displacement of the membrane is of interest to affect the terahertz signal.

Recent work on PMUTs focuses on improving their performance. This includes overcoming the limitations due to process variation during fabrication [14], providing methods on how to tune the resonant frequency of the PMUTs [6], augmenting the acoustic pressure generated by the PMUTs [2], [15] and creating dual frequency responses [16]. While these works generally use commercially available MEMS fabrication processes on silicon wafers [6], [14], [15], [17], others develop customs fabrication processes to improve the integration of PMUTs. This includes their fabrication onto flexible substrates [8], [18]. Most works focus on the fabrication process and the transducer design to improve the performance of the PMUTs. This work aims at looking at the impact of the excitation signal on the performance of PMUTs considered as nonlinear MEMS resonators by leveraging pulse shaping.

Pulse shaping can be as simple as a frequency modulation of the excitation signal which in turn results in the amplitude modulation of the displacement of the resonating device. This is a direct use of the hysteresis in nonlinear resonators, which allows the modulation of the frequency content of the signal to affect the amplitude of the signal. Conversely, the modulation of the amplitude of the excitation signal allows in turn to control of the resonant frequency of the resonator. Accordingly, a modulation in frequency of the excitation signal results in a modulation in amplitude of the velocity of the membrane. Thus, the contributions of pulse shaping can be listed as follows:

(i) enabling the tuning of the resonant frequency of the resonator using the amplitude of the excitation signal;
(ii) using the resonator at a frequency that doesn't have to be its resonant frequency;
(iii) increasing the displacement of the resonator's membrane; and
(iv) control of the decay time of the resonator.

The use of nonlinear features in MEMS resonators for pulse shaping is of great interest as, when compared to macroscopic resonators, they are more likely to have a nonlinear response [19]. Furthermore, these MEMS resonators are generally driven close to their nonlinear regime to increase their performance [20]. Finally, the use of nonlinear MUTs seems to be a trend as more and more MEMS devices are leveraging

M. Gratuze, A. Alameh and F. Nabki are with the Department of Electrical Engineering, École de Technologie Supérieure, Université du Québec, Montréal, QC H3C 1K3, Canada A. Robichaud is with the Department of Applied Sciences, Université du Québec à Chicoutimi, Saguenay, QC G7H 2B1, Canada (e-mail: mathieu.gratuze.1@ens.etsmtl.ca; abdul-hafiz.alameh.1@ens.etsmtl.ca; alexandre_robichaud@uqac.ca; frederic.nabki@etsmtl.ca).

such phenomena: accelerometers, energy harvesters, actuators, switches, and resonators [21–27]The first applications of nonlinear PMUTS for jamming applications has been presented by [28]. It should be noted that nonetheless other works are also aiming to reduce the nonlinearity of MEMS resonators [29–31].

Accordingly, this work explores the use of pulse shaping using a nonlinear MEMS resonator to enhance performance and is structured as follows: the necessary background is presented in Section II. Afterwards, simulations are presented in Section III to outline the impact of pulse shaping on a nonlinear resonator. Experimental validation is then presented in Section IV, covering the design and fabrication of the devices, the experimental test setup and the experimental results. Thereafter, Section V discusses the benefits of pulse shaping and provides a comparison to the literature. Finally, conclusions are presented in Section VI.

II. Background and Theory

A. Operating Principle of Micromachined Ultrasonic Transducers

At the micro scale, capacitive micromachined ultrasonic transducers (CMUTs) are an alternative to PMUTs. Both these device types are manufactured using MEMS fabrication processes, with a key difference being the actuation mechanism, where CMUTs are actuated using electrostatic force, while PMUTs leverage a piezoelectric actuation. Due to the experimental results presented touching on piezoelectric nonlinear resonators, this paper will mainly focus on PMUTs, but in theory pulse shaping can be applied to any type of MUTs as long as their behavior is nonlinear. It should be noted that nonlinearity can be introduced in MUTs by increasing the amplitude of the excitation.

MUTs transform an electrical signal into a mechanical signal through an sinusoidal excitation signal at a defined amplitude A and frequency ω. In the case of CMUTs, a bias DC signal also needs to be applied. Two main types of waveforms are used: pulsed waves and continuous waves. In the first case, a predefined number of periods are sent, while in the second case the transducer is continuously excited. However, the shape of the emitted mechanical signal is a function of both the applied electrical pulses and the frequency response of the transducer.

MUTs can be considered as resonators, therefore the effective frequency at which they can operate is limited by their resonant frequency, and their dynamic behavior depends on their quality factor. At resonance, the ultrasonic signal can be generated most effectively and typically, the greater the resonant frequency, the greater the temporal resolution, which can translate to imaging or ranging resolution.

A high quality factor will allow the generation of an ultrasound wave of greater amplitude which improves the maximum operating distance but reduces the spatial resolution of the transducer due to an increased decay time of the resonator in pulsed operation. Therefore, to increase the performance of ultrasonic transducers, it is of interest to design devices able to generate large acoustic signals that have a short duration or provide a solution allowing for the reduction of the decay time without reducing the quality factor.

Finally, both PMUTs and CMUTs are fabricated using microfabrication processes that result in inherent variations from device to device, which can cause variations in the resonant frequency of the resonator. Such variations decrease the sensitivity it a pitch and catch configuration, and can also require careful tuning of the excitation signal frequency to maximize output acoustic power. This warrants the development of a resonant frequency tuning mechanism to mitigate this effect.

Increasing the performance of PMUTs by generating more displacement, reducing the decay time without reducing the quality factor and providing resonant frequency tuning is considered in this work by leveraging the transducer nonlinearity via shaping of the excitation signal (i.e., pulse shaping).

B. Modeling Nonlinearities in MEMS resonators

It should be noted that for the modelling of MEMS devices, using the Duffing equation for a MEMS system (instead of the appropriate micro-beam or micro-plate model) can lead to inaccurate results. Improving the accuracy of the analytical modelling of the nonlinear behavior of MEMS devices is still of interest. Examples of such models have been presented in [32–36]. However, such models are dependent on the geometry of the MEMS device considered, and the aim of this paper is not to provide new or improved modelling methods of nonlinear MEMS devices, but focus on leveraging nonlinear effects in MEMS devices to affect their resonant behavior in pulsed excitation. Therefore, it will be considered nonetheless that the dynamic response of MEMS resonators can be analytically expressed using the Duffing equation.

In such a system, x, the deflection of one point of the resonator, can be expressed as a function of the parameters of the resonators such that the equation of motion can be written as [37]:

$$m\ddot{x} + c\dot{x} + k_0 x + k_1 x^2 + k_2 x^3 = A * F(t), \tag{1}$$

where m is the effective mass, c is the effective damping, and k_0, k_1, and k_2 represent linear, square and cubic stiffness coefficients, respectively. The deflection is also function of A, the amplitude of the excitation signal, and $F(t)$, the excitation signal. In such a system, the undamped fundamental resonant frequency f_0 is given by [37]:

$$f_0 = \frac{1}{2\pi}\sqrt{\frac{k_0}{m}}. \tag{2}$$

The quality factor, Q, can be estimated as [37]:

$$Q = \frac{\sqrt{mk_0}}{c}. \tag{3}$$

This allows the determination of the fundamental resonant frequency f_r as [37]:

$$f_r = f_0\sqrt{1 - \frac{1}{2Q^2}}. \tag{4}$$

Finally κ, the amplitude-frequency coefficient, can be expressed as [37]:

$$\kappa = \left(\frac{3k_2}{8k_0} - \frac{5k_1^2}{12k_0^2} \right) f_0. \quad (5)$$

The value of κ determines the general behavior of the system. If $\kappa > 0$, then an increase of the amplitude leads to an increase of the resonant frequency. This behavior is called spring hardening. On the contrary, if $\kappa < 0$, an increase of the amplitude leads to a reduction of the resonant frequency. This behavior is called spring softening.

Equations 1 to 5 can also be used to describe the behavior of linear devices, in this case $k_1 = k_2 = 0$, which in turns results in $\kappa = 0$ such that in such a system, the resonant frequency does not vary with the amplitude of the excitation signal.

III. Simulation Results

A. Definition of the Nonlinear Resonator

To illustrate the case at hand, and create a theoretical model, an ideal Duffing resonator has been defined H_R. For such a resonator, unitless parameters, m, c, k_0, k_1, and k_2 have been determined and are presented in Table I. This set of parameters results in f_0 = 500.01 Hz, f_r = 500.01 Hz, $Q = 314.16$ and $\kappa = 1.90$. Therefore, H_R will have a hardening type behavior.

The behavior of H_R has been simulated using MATLAB (2020B) with the ordinary differential equation solver ode45. It has then been characterized following the guidelines presented in [38]. The result of such characterization is presented in Fig. 1. Fig. 1a presents the behavior of H_R between 400 Hz and 600 Hz using three different excitation signals with a constant amplitude ($A = 20$). In the first case, the frequency is continuously increased and this has been named a continuous sweep forward (CSF) signal. In the second case, the frequency is continuously decreased and this has been named a continuous sweep backward (CSB) signal. And in the third case, the behavior is characterized for each frequency discretely, and this has been named a pulsed sweep (PS) signal. The impact of varying the amplitude of the excitation signal on the maximal amplitude frequency (F_{mv}) is shown in Fig. 1b. The maximal amplitude of $x(t)$ is shown in Fig. 1c for different excitation amplitudes. This behavior was expected as it is in agreement with the behavior of a hardening type nonlinear resonator as predicted by $\kappa = 1.90$.

The characteristics of H_R have been extracted for three values of A of 10, 15 and 20. In particular, the maximum amplitude of $x(t)$ and value of F_{mv} were extracted. These results are compiled in Table II. While these results have been extracted using simulation of the theoretical model, work in [36] has shown that it possible to extract these values analytically from eq.1. As seen from this table, the amplitude of the excitation signal can be used as a simple tuning mechanism of the value of (F_{mv}).

TABLE I: Characteristics of the simulated resonator

	m	c	k_0	k_1	k_2	f_0(Hz)	f_r(Hz)	Q	κ
H_R	1×10^{-4}	0.001	987	0	10	500.01	500.01	314.16	1.90

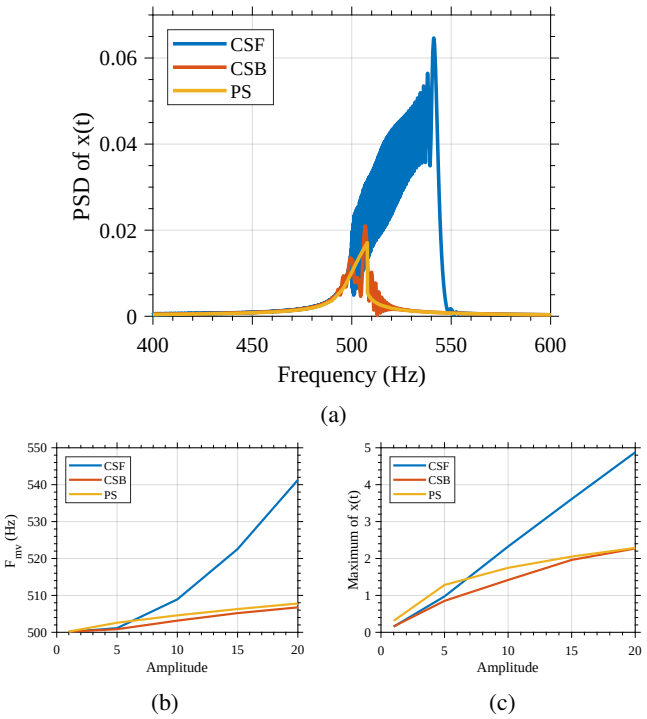

Fig. 1: (a) Impact of the type of excitation signal with a constant amplitude on the behavior in frequency, (b) impact on F_{mv} of modifying the excitation amplitude, and (c) the impact on maximal amplitude of $x(t)$ of modifying the excitation amplitude.

In the case of nonlinear resonators of the hardening type, increasing the amplitude of the excitation signal can act as a frequency tuning mechanism. As shown in Fig. 1 and Table II, increasing the value of A leads to an increase of F_{mv}. When H_R is excited with a CSF type excitation, the maximum amplitude of $x(t)$ reached is greater than the one that can be leveraged using a PS or CSB type excitation, and this is also true for the variation in F_{mv}.

It should be noted that while this demonstration has been made using an ideal nonlinear resonator with a hardening type response, it is possible to do a similar exercise with an ideal nonlinear resonator with a softening type response. In such a case, increasing the amplitude of the excitation signal reduces the value of F_{mv} as softening type resonators are characterized by having $\kappa < 0$.

TABLE II: Performance of the simulated resonator

	Amplitude of excitation	CSF	CSB	PS
Maximum of $x(t)$	10	2.324	1.417	1.747
	15	3.610	1.962	2.052
	20	4.877	2.270	2.287
F_{mv} (Hz)	10	508.9	503.2	504.6
	15	522.6	505.2	506.3
	20	541.3	506.8	507.8

B. Increasing the Maximum Amplitude of $x(t)$

Nonlinear resonators exhibit a hysteresis phenomenon that is the cause for which the CSF type excitation can yield a greater maximum amplitude of $x(t)$ than the PS and CSB excitations in the case of a hardening type resonator. In the case of a softening type resonator, the CSB type excitation will yield a greater maximum amplitude of $x(t)$. Therefore, to increase the maximum amplitude of $x(t)$ of the resonator, it is possible to exploit such hysteresis.

As such, a modified excitation signal has been created. This excitation signal has the following 4 phases:

1) Between $t = 0$ and $t = t_1$ no excitation is provided.
2) Between $t = t_1$ and $t = t_2$ the frequency of the excitation is gradually increased from $f = F_1$ to $f = F_2$.
3) Between $t = t_2$ and $t = t_3$ the frequency of the excitation is kept constant at $f = F_2$.
4) Between $t = t_3$ and $t = t_4$ no excitation is provided.

The amplitude of the excitation signal is kept constant during phases 2 and 3. The maximum amplitude of $x(t)$ should be stable and attained during phase 3 at $f = F_2$. To illustrate the full benefits of this excitation method, five excitation signal types (**(a)** to **(e)**) have been defined, with the following purposes:

- **Signal (a):** show the benefits of pulse shaping.
- **Signal (b):** show the frequency tuning benefits of pulse shaping.
- **Signal (c):** show the limits of conventional (single frequency) excitation.
- **Signal (d):** show the benefits of excitation signal **(a)**.
- **Signal (e):** show the benefits of excitation signal **(b)**.

Such an excitation signal then needs to be tailored for each specific nonlinear resonator, and for each excitation amplitude, as the amplitude of the excitation signal has an impact on the frequency behavior of the nonlinear resonator. The parameters $t_1 = 0.5\,\mathrm{s}$, $t_2 = 1.5\,\mathrm{s}$ and $t_3 = 3.0\,\mathrm{s}$ have been kept constant for all excitation signals. It should be noted that each phase has a minimal suitable duration. This minimal duration is a function of the parameters of the resonators, among them Q-factor and the resonant frequency. If the minimal duration of each phase is not respected, then the benefits of the excitation signal will not be exhibited.

The parameters of each excitation signal type **(a)** to **(e)** is presented in Table III. It should be noted that the implementation of excitation signals type **(a)** and **(b)** should be carefully created as a discontinuity in time in between phase 2 and phase 3 in such a signal will be detrimental to the performance.

Table III also summarizes the properties of each excitation signal type. Excitation signal types **(c)**, **(d)** and **(e)** are a continuous sine waves at a defined frequency as $F_1 = F_2$. It should be noted that the frequency of signal **(c)** is of $507\,\mathrm{Hz}$, which is greater than the $500.01\,\mathrm{Hz}$ resonant frequency of $\mathrm{H_R}$; this discrepancy is explained by the fact that $\mathrm{H_R}$ is a hardening type nonlinear resonator. Using excitation signal type **(a)** allows an increase of the maximum amplitude of $x(t)$ of 210% compared to the maximum amplitude of $x(t)$ obtained with excitation signal type **(c)** and 4075% when compared with the maximum amplitude of $x(t)$ obtained with excitation signal type **(d)**.

TABLE III: Characteristics of the different simulated excitation signal types

Signal type	Amplitude	F_1	F_2	Maximum amplitude of $x(t)$
(a)	20	480	541	4.810
(b)	20	480	530	4.130
(c)	20	507	507	2.287
(d)	20	541	541	0.118
(e)	20	530	530	0.164

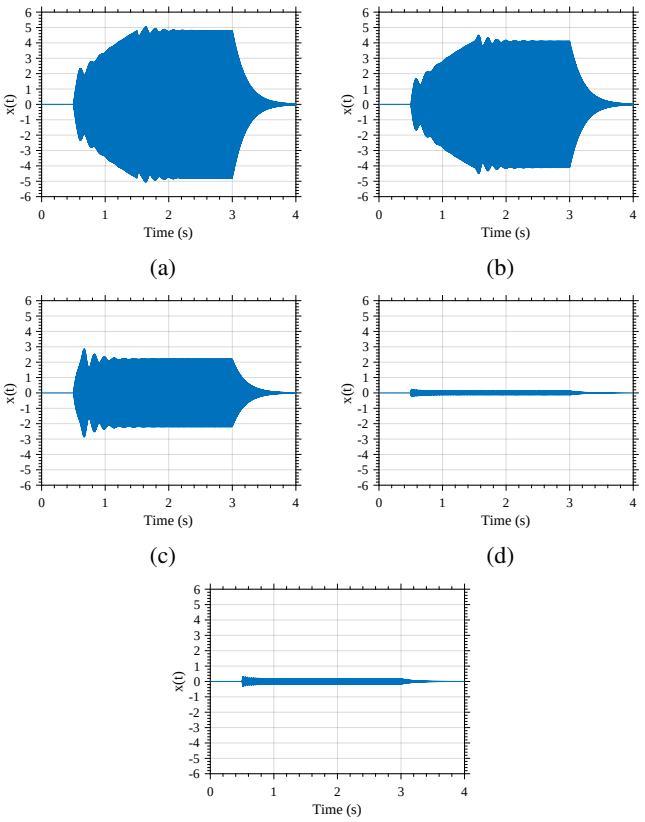

Fig. 2: Impact of the excitation signal type on the amplitude of $x(t)$. Each sub-figure (**(a)** to **(e)**) corresponds to an excitation signal defined in Table III.

The use of such excitation signals also allows the use of a frequency that is not the resonant frequency while still displaying a greater maximum amplitude of $x(t)$. This is illustrated through excitation signal type **(b)** that allows for an 180% increase of the maximum amplitude of $x(t)$ compared to that achieved with excitation signal type **(c)**. Moreover, in comparison to the maximum amplitude of $x(t)$ obtained with excitation signal type **(e)**, this represents a relative increase of 2518%.

The impact of each of these excitations on $\mathrm{H_R}$ is illustrated in Fig. 2, showing the amplitude of $x(t)$ of the resonator versus time. In this figure, the increase in maximum amplitude of $x(t)$ is clearly seen when the devices are excited using excitation

signal types **(a)** and **(b)**. However, it is also apparent that excitation signal types **(a)** and **(b)** need some time before reaching the maximum amplitude of $x(t)$. This time is can be detrimental to the performances of devices such as PMUTs, as it decreases axial resolution; therefore, efforts should be made to decrease this time.

C. Reduction of the Excitation Signal Duration

To reduce the time needed before reaching the maximum amplitude of $x(t)$, it is necessary to reduce the difference between the frequencies F_1 and F_2. This reduction is possible thanks to the unique frequency behavior of nonlinear resonators. In such behavior, as illustrated in Fig. 3 it is possible to observe two strong discontinuities. In the case of a hardening type resonator, these discontinuities can be observed when the frequency decreases from $f = F_1$ to $f = F_2$, and when the frequency increases from $f = F_3$ to $f = F_4$. The first one leads to a strong increase of the amplitude of $x(t)$ when $f = F_A$, while the second one to a strong decrease of the amplitude of $x(t)$ of the resonator when $f = F_B$.

Using such information, an optimized excitation signal has been created. This excitation signal has the following 6 phases:

1) Between $t = 0$ and $t = t_1$ no excitation is provided,
2) Between $t = t_1$ and $t = t_2$ the frequency of the excitation is gradually decreased from $f = F_1$ to $f = F_2$,
3) Between $t = t_2$ and $t = t_3$ the frequency of the excitation is gradually increased from $f = F_2$ to $f = F_3$,
4) Between $t = t_3$ and $t = t_4$ the frequency of the excitation is kept constant at $f = F_3$,
5) Between $t = t_4$ and $t = t_5$ the frequency of the excitation is gradually increased from $f = F_3$ to $f = F_4$,
6) Between $t = t_5$ and $t = t_6$ no excitation is provided,

The amplitude of the excitation signal is kept constant during phases 2 to 5. The maximum amplitude of $x(t)$ should be stable and provided during phase 4 at $f = F_3$. This excitation signal is illustrated in Fig. 4. It should be noted that the implementation of excitation signal types **(a)** and **(b)** should be carefully created as a discontinuity in time in between phase 2 and phase 3, in between phase 3 and phase 4 or in between phase 4 and phase 5 will be detrimental to performance. Indeed, if such a discontinuity in time is present, then the nonlinear resonator will be unable to reach the maximum amplitude.

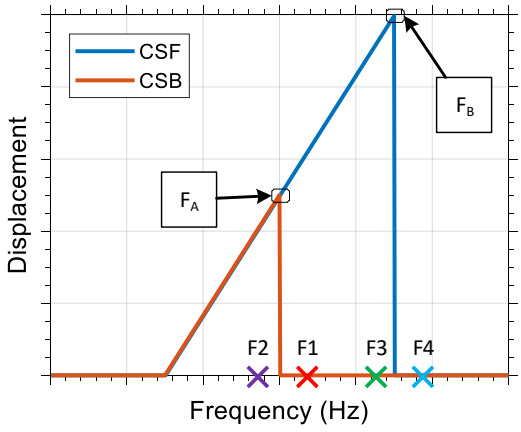

Fig. 3: Illustration of the influence of the direction of the sweep in frequency on the frequency response of a typical hardening resonator. The frequencies F_1 to F_4, F_A and F_B are identified.

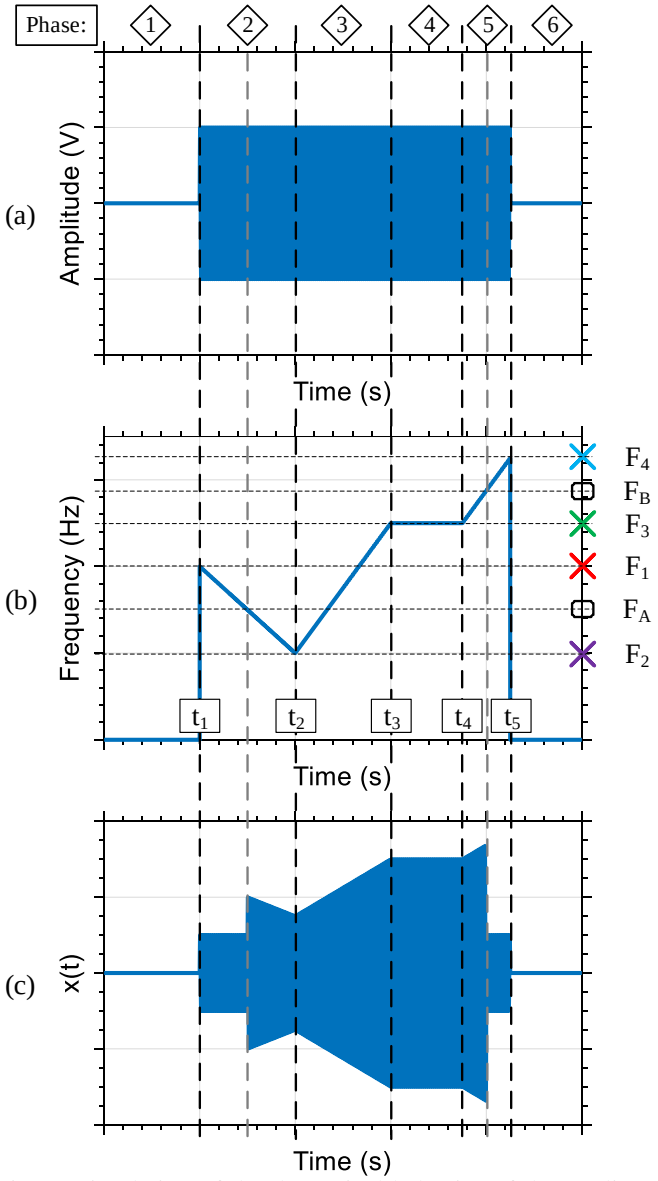

Fig. 4: Simulation of the theoretical behavior of the nonlinear resonator when excited using pulse shaping, in (a) the excitation signal as well as the different phases are shown, in (b) the frequency content of the excitation signal is presented with frequencies F_1 to F_4, F_A and F_B identified, and finally in (c) the expected behavior of the nonlinear resonator is presented.

Fig. 4 shows the expected behavior of the nonlinear resonator. The discontinuities in amplitude of $x(t)$ are observed at $t = t_A$ when $f = F_A$ and $t = t_B$ when $f = F_B$. The use of the first discontinuity allows a strong increase of the amplitude of $x(t)$, while the second one allows a strong decrease of the amplitude of $x(t)$. This second discontinuity will be used to control the decay of the resonator. This is illustrated in Fig. 4 as well.

The validation of the impact of such an excitation signal will be performed experimentally using a nonlinear MEMS resonators. It should be noted that while this demonstration has been made using an ideal nonlinear resonator with a hardening type response, it is possible to do a similar exercise with nonlinear resonator with a softening type response. In such a case, the relationship between the excitation frequencies is slightly different to take advantage of both discontinuities in the frequency behavior of softening type resonators. In the case of a hardening type resonator, the relationship between F_1, F_2, F_3, F_4, F_A and F_B is:

$$F_2 < F_A < F_1 < F_3 < F_B < F_4 \tag{6}$$

And in the case of a softening type resonator, this relationship becomes:

$$F_4 < F_A < F_3 < F_1 < F_B < F_2 \tag{7}$$

In both cases, the maximum amplitude of $x(t)$ will be stable and provided during phase 4 at $f = F_3$.

IV. Experimental Validation

A. Design and Fabrication

To experimentally validate the potential of pulse shaping to improve the performance of nonlinear MEMS resonators, two devices have been designed and fabricated. These nonlinear resonators are based on the Squared Daisy structure presented in [39]. One interesting property of this structure is its ability leverage both types of nonlinear stiffness (*either* spring softening *or* spring hardening) depending on the anchoring scheme used, as shown in [38]. This property is especially of interest in this case as it will allow the demonstration of pulse shaping for nonlinear MEMS resonators exhibiting either *either* spring softening *or* spring hardening.

The MEMS resonators have been fabricated using the commercial PiezoMUMPs process from MEMSCAP (Crolles, France). This process is a piezoelectric-based MEMS process that has been used in the literature to create MEMS resonators, energy harvesters, sensors, and ultrasonic transducers [6], [14], [39–42].

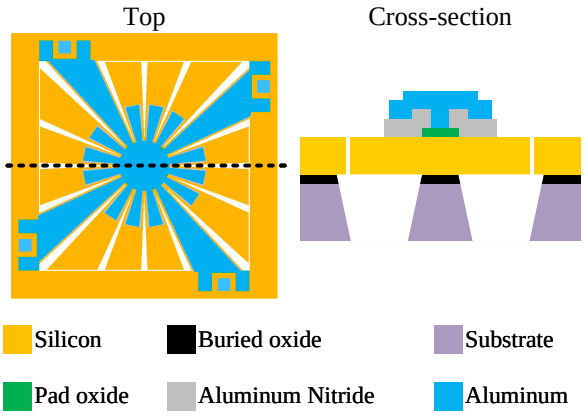

Fig. 5: Top view and cross section of the MEMS softening type resonator.

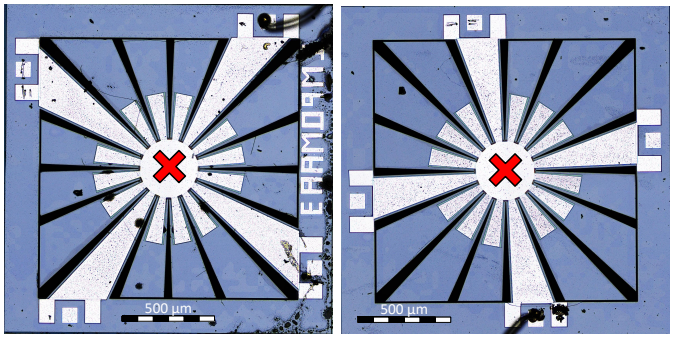

(a) (b)

Fig. 6: Micrograph of the fabricated (a) softening type resonator and (b) hardening type resonator. The measurement point used for characterisation is outlined.

The anchoring of these nonlinear MEMS resonators has been chosen so that one of the resonators exhibits a softening type response and the other one a hardening type response. Each design occupies an area of 1700 by 1700 µm. Fig. 5 provides both a cross-section and top view of the MEMS structure, for the softening type device. All of the layers used in the process are clearly identified. Further details regarding the fabrication process can be found in [43]. The membrane of the resonators is made of a 10 µm-thick silicon layer (Si) in the (001) orientation. This layer also acts as the bottom electrode, as it has been doped. The piezoelectric material is a 0.5 µm-thick layer of aluminum nitride (AlN). This layer will allow the generation of the strain to displace the membrane. The top electrode is made of the combination of a stack of 20 nm-thick chromium (Cr) and 1 µm thick aluminum (Al). Electrical isolation between the two electrodes is provided either by the AlN layer or by a 0.2 µm-thick layer of silicon dioxide (SiO_2). Upon reception of the device from the foundry, no post-processing step was applied to the devices.

Pictures of the realized structures are shown in Fig. 6. In this figure, the measurement point, in the center of the proof mass is clearly indicated. This measurement point will be kept constant for all further experiments. In Fig. 6(a) the resonator has a softening type response, and in Fig. 6(b) it has a hardening type response. From this point forward, these resonators will be referred to as softening type resonator (STR) and hardening type resonator (HTR), respectively. The mode shape of the realized structures is presented in the appendix.

B. Description of the Experimental Test Setup

To characterize the behavior of the MEMS resonators under the different excitation signal types, the following approach was carried out. Results were obtained by electrically driving the transducers and measuring their mechanical response using a vibrometer from Polytec (Irvine, CA, USA). The vibrometer is used to measure the velocity of the measurement point on the devices, as outlined previously. The test setup is presented in Fig. 7. It is comprised of the following components: a data management system, the vibrometer controller (OFV-2570) and the laser unit (OFV-534). The electrical excitation is provided by a function generator type 33250A from

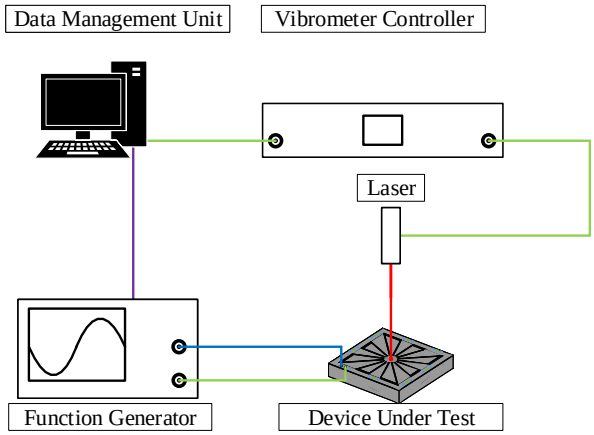

Fig. 7: Schematic of the vibrometer test setup.

Keysight (Santa Rosa, CA, USA). This function generator is controlled using MATLAB (2020B) to vary the frequency and amplitude of the excitation signal.

The sampling frequency of the measurements made with the vibrometer was set to $2.56\,\mathrm{MHz}$. This frequency was chosen to provide large oversampling of the signal (as the operating frequency of the device is below $10\,\mathrm{kHz}$), and thus allow precise observation of the velocity of the measurement point shown in Fig. 6.

C. Characterization of the Devices

As shown in section III-C, to exploit the full capability of pulse shaping, proper characterization of the devices needs to be conducted. Due to the amplitude dependent nonlinear behavior of the MEMS resonator, the characterization of the devices is more complex than the characterization of a linear MEMS resonator. Work in [38] provides further details regarding the characterization methodology of the devices. This includes the generation of the excitation waveforms (PS, CSF and CSB), and their impact on the experimental characterization of the nonlinear MEMS resonators.

The behavior in frequency of the resonators presented in section IV-A has been characterized using the test setup presented in Fig. 7. A pulsed sweep (PS) signal is used along with continuous sweeps in both the forward (CSF) and backward (CSB) direction. This characterization has been made when the excitation signal amplitude is equal to $10\,\mathrm{V}$ and $20\,\mathrm{V}$. The results are summarized in Table IV. The impact of the amplitude of the excitation signal on the value of F_{mv} is highlighted by the presence of the line named ΔF_{mv}. This variation validates the first tuning mechanism used in pulse shaping: the amplitude of the excitation signal, A, has a direct impact on the value of F_{mv}. As explained and simulated in section III-C, the impact of the signal sweep type used to extract F_{mv} for each device, and the impact of the amplitude of the excitation signal (as explained in section III) can be observed. Changing the amplitude of the excitation signal results in a variation of F_{mv}, such that for the STR, increasing the amplitude of the excitation signal decreases F_{mv} as $\kappa < 0$.

TABLE IV: Summary of the characteristics of both resonators types for different excitation signal sweeps

	Excitation voltage (V)	STR PS	STR CSF	STR CSB	HTR PS	HTR CSF	HTR CSB
F_{mv} (Hz)	10	3970	3969	3854	7800	7812	7797
	20	3920	3918	3638	7910	8058	7879
ΔF_{mv} (Hz)	–	-50	-51	-216	110	246	82

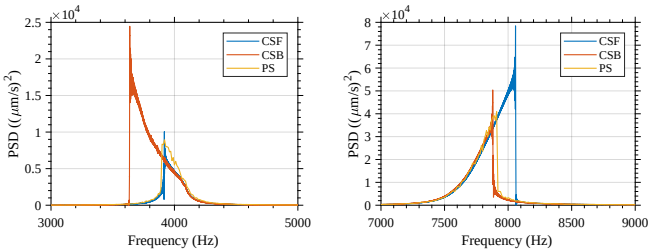

(a) (b)

Fig. 8: Visualization of the influence of the direction of the frequency sweep on the frequency response of: (a) softening resonator (STR) (b) hardening resonator (HTR). Reprinted from [38].

On the other hand, F_{mv} increases for the HTR for an increased amplitude since $\kappa > 0$.

Graphical visualization of these results are shown in Fig. 8a for the STR and in Fig. 8b for the HTR. These figures shows the power spectrum density of the velocity of the device when the device is excited with the three different signal sweep types used. It should be noted that while the simulations were performed using the amplitude of $x(t)$, the experimental results show the velocity ($\dot{x}(t)$) as extracted by the vibrometer controller. Nonetheless the results can be relied upon to characterize the devices as the velocity it is the derivative of the displacement. Note that while frequencies F_A and F_B have been determined experimentally, it is possible to determine them analytically as shown in [36].

D. Description of the Excitation Signals

The excitation signals have been devised following the instructions presented in section III-C. To experimentally illustrate the full benefits of this excitation method, five excitation signals have been defined with the same purposes as those proposed in section III-B and using the scheme outlined in section III-C.

Such excitation signals then need to be tailored for each specific nonlinear resonator, and for each amplitude of excitation, as the amplitude of the excitation signal has an impact on the frequency behavior of the resonator. The description of each excitation signal type (**(a)** to **(e)**) is presented in Table V. For these excitation signals, the parameters T_1 to T_6 have not been kept constant, but the rate at which the excited frequency varies has been kept constant. This rate has been defined at $1\,\mathrm{kHz\,s^{-1}}$.

E. Impact of Pulse Shaping

The impact of each of the excitation signals described in the previous section on the velocity of the HTR and STR

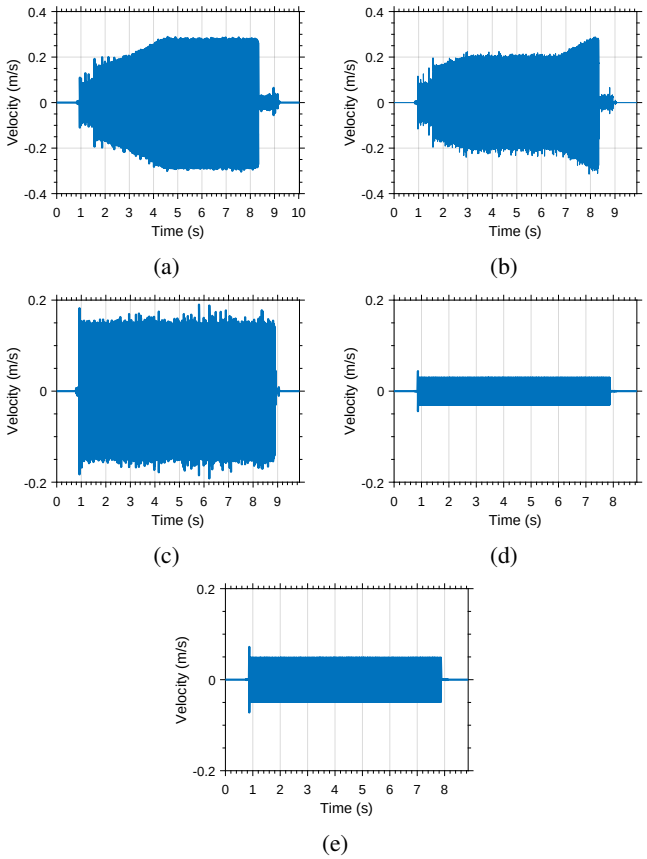

Fig. 9: Impact of the type of excitation on the displacement of the STR. Each sub-figure (**(a)** to **(e)**) corresponds to an excitation signal type as defined in Table V.

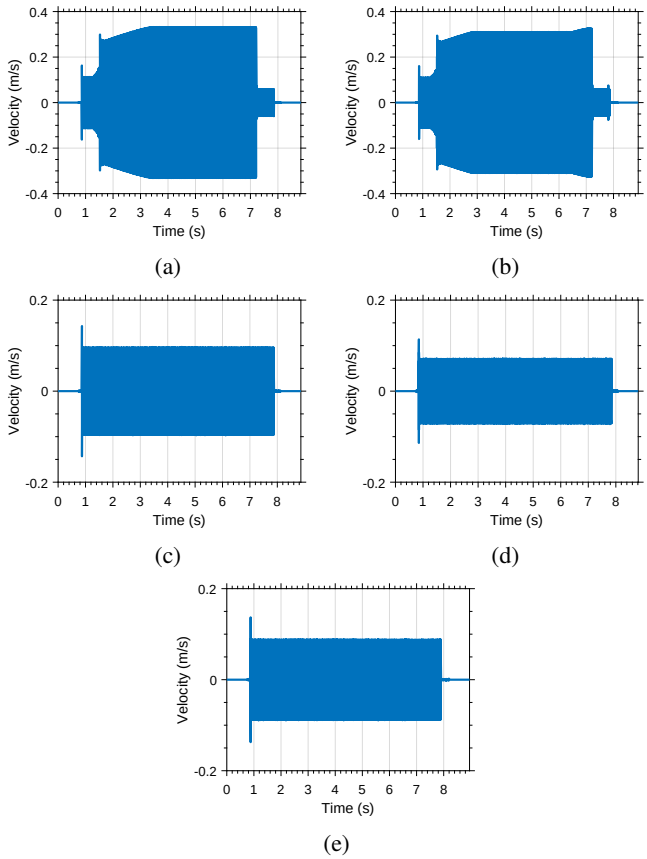

Fig. 10: Impact of the type of excitation on the displacement of the HTR. Each sub-figure (**(a)** to **(e)**) corresponds to an excitation signal type as defined in Table V.

is illustrated in Fig. 9 for the STR and in Fig. 10 for the HTR. The envelope of the displacement of the resonators is in agreement to the predicted behavior shown in Fig. 4. This is particularly visible in the case of excitation signal type **(b)**, as presented in Fig. 9b for the STR and Fig. 10b for the HTR. The agreement is also seen when the frequency of the excitation signal stays constant as illustrated in Fig. 9c to Fig. 9e and Fig. 10c to Fig. 10e, comparing well to the behavior shown in Fig. 2c to Fig. 2e.

The velocity in steady state for both resonator types has been extracted for each excitation signal, and is presented in Table V. Notably, due to the pulse shaping, excitation signal type **(a)** allows for a velocity that is 191% higher for the STR and 348% higher for the HTR, as compared to what is obtained with signal type **(c)**. When compared to the results achieved using signal type **(d)**, this represents an increase of 907% and 474% for the STR and HTR, respectively. This outlines the advantage of the proposed pulse shaping.

TABLE V: Characteristics and velocity performance of the different experimental excitation signals

	Signal type	F_1 (Hz)	F_2 (Hz)	F_3 (Hz)	F_4 (Hz)	Maximal velocity ($\mathrm{m\,s^{-1}}$)
STR	**(a)**	3910	3920	3640	3630	0.2712
	(b)	3910	3920	3800	3630	0.1954
	(c)	3920	3920	3920	3920	0.1417
	(d)	3640	3640	3640	3640	0.0299
	(e)	3800	3800	3800	3800	0.0489
HTR	**(a)**	7850	7845	8015	8035	0.3313
	(b)	7850	7845	7950	8035	0.3093
	(c)	7910	7910	7910	7910	0.0950
	(d)	8015	8015	8015	8015	0.0698
	(e)	7950	7950	7950	7950	0.0880

The ability to use nonlinear resonators outside of their resonant frequency is also clearly highlighted. This can be seen with excitation signal type **(b)** that allows for a velocity that is 138% higher for the STR and 325% higher for the HTR compared to the displacement obtained with signal type **(c)**. When comparing to signal type **(e)** a velocity increase of 400% for the STR and 351% for the HTR is observed.

Accordingly, the experimental behavior is in agreement with the predictions formulated in section III-C. Therefore, the use of pulse shaping enables a higher velocity than what is possible when operating the device without pulse shaping at the resonant frequency. It also enables the operation of the nonlinear MEMS resonator over a wider range of frequencies.

Another benefit of pulse shaping is the ability to control the decay time of the resonator. This can be done by leveraging the sharp discontinuities in the frequency response of the nonlinear devices during phase 5 described in section III-C. The effect is shown in Fig. 11. However, the duration of this phase needs to be carefully selected. If the duration of phase 5 is too long, rebounds will appear in the displacement of the device during the decay. This behavior has been measured experimentally as

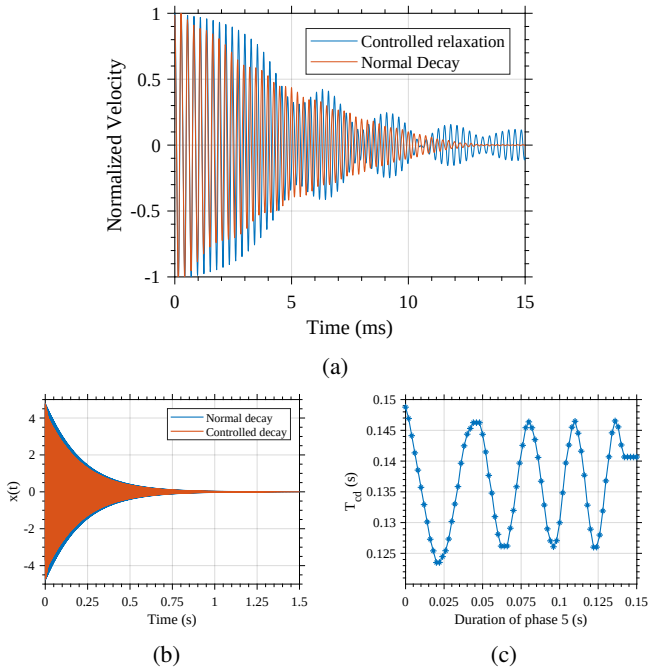

Fig. 11: Visualisation of the impact of the excitation method on the decay of the device: (a) measurement, (b) simulation, and (c) simulation of the effect of varying the duration of phase 5 on T_{cd}.

shown in Fig. 11a and simulated using H_R. It should be noted that experimentally a rebound-free decay is hard to obtain, this is mostly due to the current limit of the experimental test setup.

Simulations using H_R have been performed to grasp the impact of the duration of phase 5 on the decay time of the resonator. The time of constant decay T_{cd} has been defined as the time needed to reduce the amplitude of the displacement by 50%. Under no phase 5 excitation, T_{cd} has been simulated at $148.8\,\mathrm{ms}$. However, simulations have shown that if the duration of phase 5 is equal to $20\,\mathrm{ms}$ then T_{cd} is reduced to $123.5\,\mathrm{ms}$, which represents a 17% reduction of T_{cd}. This case is illustrated in Fig. 11b. In this figure, it is clear that the controlled decay is faster than the normal decay of the resonator.

The effect of the variation of the duration of phase 5 on the value of T_{cd} is clearly shown in Fig. 11c. This highlights the benefits of pulse shaping as a way to control the value of T_{cd}, as the use of the phase 5 allows a reduction of T_{cd}. The value of T_{cd} under normal decay occurs when the duration of phase 5 is equal to $0\,\mathrm{ms}$ and is greater than all the other values obtained when varying the duration of phase 5.

It should be noted that the duration of phase 5 should be carefully controlled to exhibit optimal decay as if the duration of this phase is greater than the normal decay, then the value of T_{cd} is constant and in the case of H_R is equal to $140.7\,\mathrm{ms}$, which represents a reduction of T_{cd} of 5.4%. A longer duration for phase 5 is not recommended as then rebounds will happen as shown experimentally in Fig. 11a. It should be noted that the optimal duration for each phase of the excitation signal is dependant of the intrinsic parameters of each resonator.

V. Discussion

In this section, a discussion of the experimental results presented in section IV-E is presented. As stated previously, this excitation method is to the best knowledge of the authors a first for MEMS resonators. It is expected that the main application of pulse shaping as described here will be to increase the performance of MUTs.

The results presented in Fig. 9 and Fig. 10 are not yet comparable to typical pulsed wave excitation as the duration of the pulse is too long (i.e. about $8\,\mathrm{s}$). However, it is possible to compress these signals in the time domain by increasing the rate at which the frequency varies in phase 2 and phase 5 of the excitation signal. It should be noted there is a limit to the compression of these signals in the time domain as each phase has a minimal duration. Currently no analytical method is available to determine the minimal excitation duration. It is thus is determined qualitatively by setting it to a relatively large value and then gradually reducing it until the response of the resonator does not exhibit the benefits of the pulse shaping. This minimal duration is a function of the parameters of the resonators among them Q and the resonant frequency of the resonator and of the excitation signal (amplitude, and frequency content). If the minimal duration of each phase is not respected, then the benefits of the excitation signal will not be exhibited. However, the results obtained using the pulse shaping methodology are comparable to the continuous wave excitation while providing enhanced displacement and thus increased acoustic power in the context of MUTs, as once the maximum displacement is reached, this state is stable. This paves the way to the use of nonlinear resonators for the emission of ultrasonic signals at higher relative output power.

Several techniques have been developed to improve the performances of MUTs. As such, [6] and [14] have presented methods on how to limit the effects of process variation on the resonant frequency of MUTs, and as a result a passive frequency tuning method is proposed. Work in [4] presents the use of a biasing signal to exploits two resonant modes with closely spaced natural frequencies near $175\,\mathrm{kHz}$, which also allows a relative control of the decay time of their resonator. Work in [44] takes advantage of a DC bias voltage in the piezoelectric layer to produce a controllable stress, which in turn allows relative control of the resonant frequency of their ultrasonic transducer. Other works such as [15] and [45] present layout methods on how to improve the displacement of the membrane of the UTs. Work in [46], presents the use of an actuator to reduce and control the decay time of the resonator by using electrostatically activated dampers. Work in [47] and [48] focus on reducing the decay time of PMUTs, where [47] presents the benefits of phase shifting the excitation signal, while [48] presents the benefits of a transfer function-based ring-down suppression system. Both succeed in significantly reducing the decay time of PMUTs. Finally [49] and [50] present the application of direct modulation which is traditionally used in RF systems to PMUTs. While they do not report an increase of the displacement of the membrane of the

TABLE VI: Comparison of the proposed method with the literature

	Mechanism employed	Tuning of the operating frequency	Increase of the maximal velocity	Control of the decay time	Non-linear use of the resonator
[4]	DC bias	**Yes** (active)	No	**Yes** (82%)*	No
[6]	Post-processing	**Yes** (passive)	No	No	No
[14]	Layout	**Yes** (passive)	No	No	No
[15]	Layout	No	**Yes** (203%)	No	No
[44]	DC bias	**Yes** (active)	No	No	No
[45]	Layout	No	**Yes** (300%)*	No	No
[46]	Actuator	**Yes** (active)	No	**Yes** (75%)*	No
[47]	Phase shift	No	No	**Yes** (85%)*	No
[48]	Transfer function	No	No	**Yes** (93%)	No
[49], [50]	Direct modulation	No	**Yes** (300%)*	No	No
This work	Pulse shaping	**Yes** (active)	**Yes** (up to 348%)	**Yes** (5.4%)	**Yes**

*estimation

PMUTs, they report an increase of the signal-to-noise ratio level and communication range of about 300% each. These results are compiled and compared with this work in table VI.

It should be noted that the strategies presented in [4], [47], [48] and this work focus on reducing the decay time of the transmitter and in a pulse-echo scenario, and that the resolution can be impacted by the Q-factor of the receiver. It should be noted that the issue of having a rebound-free decay was also encountered in the work presented by [47] and [48], and to the best knowledge of the authors, no strategies to produce a rebound-free decay have been presented yet in the literature.

While it should be possible to combine the results from these works into a single working device, to the best knowledge of the authors, no such device has been proposed in the literature. While, on the other hand, pulse shaping allows the use any existing resonator in a nonlinear regime to increase the amplitude of the displacement and reduce the decay time of such a resonator. Furthermore, it should be noted that the pulse shaping proposed here enables the operation of nonlinear resonators over a wider range of frequencies, while still attaining larger displacement (and velocity) than the traditional excitation methods that rely on linear behavior. These properties have been validated using both a simulated theoretical model and experimental data of fabricated devices.

It should be noted that while in this work a function generator has been used, a voltage-controlled oscillator (VCO) or a digital-to-analog Converter (DAC) can be used to generate excitation signals described in Fig. 4 in a more compact fashion. A dedicated driving integrated circuit could also be proposed in order to leverage the increased integration potential with the resonator.

Future work will focus on achieving amplitude modulation in the generation of the signal. This should allow an improvement of the control of the turn-on and decay time of the devices. However, this will increase the complexity of the generation of the excitation signal, as changing the excitation amplitude changes the frequency behavior of the nonlinear device, as explained in section III. Efforts will also focus on the experimental implementation of such a method on CMUTs and PMUTs arrays with much higher operating frequencies. This will allow for further validation of the method, and the use a higher resonant frequency device will allow for shorter pulses in the time domain. The devices studied in this work operate at frequencies below $10\,\mathrm{kHz}$ and the use of a CMUTs or PMUTs device operating in the MHz range will allow for much shorter excitation duration.

VI. Conclusion

In this paper, a nonlinear pulse shaping methodology which allows an increased displacement and velocity of nonlinear resonators has been presented and validated using simulation and experimental results using nonlinear MEMS piezoelectric resonators. The proposed pulse shaping is based on the frequency modulation of the excitation signal, leveraging the nonlinear frequency behavior. This in turn results in an amplitude modulation of the displacement of the resonator. Pulse shaping can thus be applied to improve the performance of resonators by using them in their nonlinear regime. The benefits of nonlinear pulse shaping were shown to increase the displacement and therefore velocity of the device (i.e., up to 348% here). Nonlinear pulse shaping also allows the operation of the resonator at a wider range of frequencies (i.e., here in a range of a few hundred Hz) while still providing improved results compared to the traditional excitation methods. Finally, pulse shaping allows a relative control of decay time of the resonator.

Accordingly, this works paves the way toward the nonlinear excitation of MEMS resonant devices to enhance their properties by specific engineering of the excitation signal, potentially enabling improved metrics such as increased range of ultrasonic transducers and increased axial resolution in ultrasonic imaging applications.

Appendix

The vibrometer test setup presented in Fig. 7 has been used to experimentally characterize the mode shape of each studied resonator variant. To this end, a 50 x 50 points grid has been carefully defined using a positioning controller type Corvus Evo from Physik Instrumente (PI) (Karlsruhe, Germany) and

2 positioners type VT-80 Linear Stage from PI. Thereafter, using this data, the amplitude of the velocity at each point was used to reconstruct the mode shape of the device. The experimentally measured mode shapes of the STR and the HTR are presented in Fig. 12 and Fig. 13, respectively, outlining the motion of the center mass and free and clamped supports as a function of the phase.

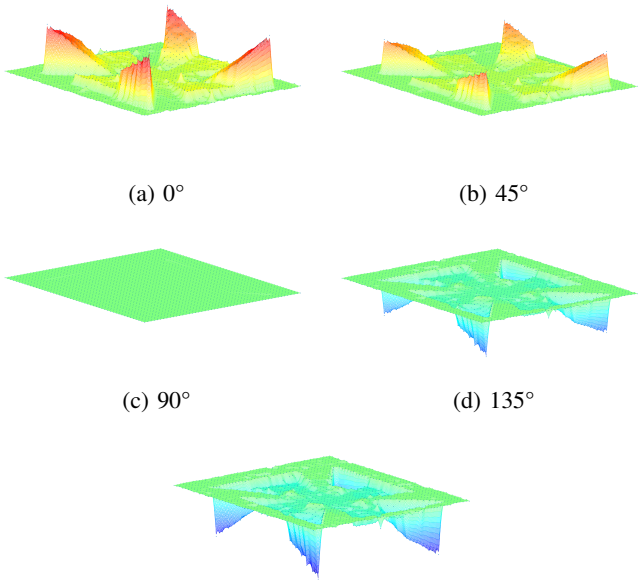

(a) 0° (b) 45°

(c) 90° (d) 135°

(e) 180°

Fig. 12: Visualisation of the mode shape of the STR as a function of the phase (between 0° and 180°).

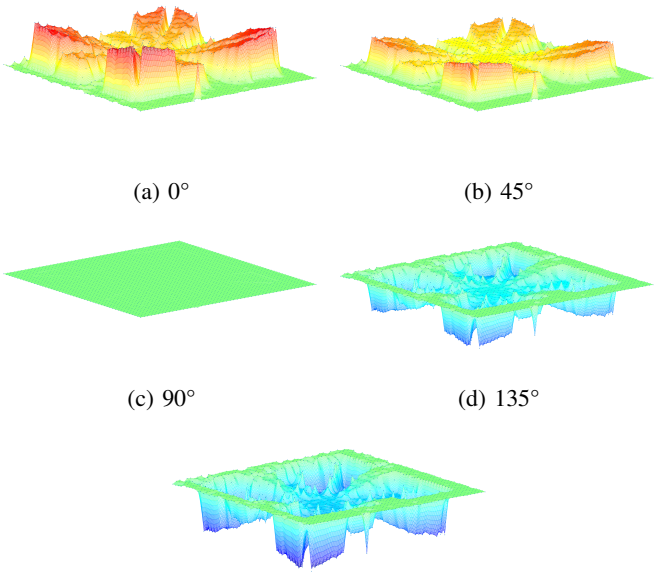

(a) 0° (b) 45°

(c) 90° (d) 135°

(e) 180°

Fig. 13: Visualisation of the mode shape of the HTR as a function of the phase (between 0° and 180°).

ACKNOWLEDGEMENT

The authors would like to thank CMC Microsystems for providing the layout design tools and enabling device fabrication, and the Natural Sciences and Engineering Research Council (NSERC) of Canada for funding of this project.

REFERENCES

[1] D. E. Dausch, J. B. Castellucci, D. R. Chou, and O. T. von Ramm, "Theory and operation of 2-D array piezoelectric micromachined ultrasound transducers," *IEEE Transactions on Ultrasonics, Ferroelectrics, and Frequency Control*, vol. 55, no. 11, pp. 2484–2492, Nov. 2008.

[2] F. Akasheh, J. Fraser, S. Bose, and A. Bandyopadhyay, "Piezoelectric micromachined ultrasonic transducers: modeling the influence of structural parameters on device performance," *IEEE Transactions on Ultrasonics, Ferroelectrics, and Frequency Control*, vol. 52, no. 3, pp. 455–468, Mar. 2005.

[3] P. Muralt, N. Ledermann, J. Paborowski, A. Barzegar, S. Gentil, B. Belgacem, S. Petitgrand, A. Bosseboeuf, and N. Setter, "Piezoelectric micromachined ultrasonic transducers based on PZT thin films," *IEEE Transactions on Ultrasonics, Ferroelectrics, and Frequency Control*, vol. 52, no. 12, pp. 2276–2288, Dec. 2005, conference Name: IEEE Transactions on Ultrasonics, Ferroelectrics, and Frequency Control.

[4] Y. Kusano, Q. Wang, R. Q. Rudy, R. G. Polcawich, and D. A. Horsley, "Wideband air-coupled PZT piezoelectric micromachined ultrasonic transducer through DC bias tuning," in *2017 IEEE 30th International Conference on Micro Electro Mechanical Systems (MEMS)*, Jan. 2017, pp. 1204–1207.

[5] C. Fei, C. T. Chiu, X. Chen, Z. Chen, J. Ma, B. Zhu, K. K. Shung, and Q. Zhou, "Ultrahigh Frequency (100 MHz–300 MHz) Ultrasonic Transducers for Optical Resolution Medical Imagining," *Scientific Reports*, vol. 6, no. 1, p. 28360, Jun. 2016, number: 1 Publisher: Nature Publishing Group. [Online]. Available: https://www.nature.com/articles/srep28360

[6] A. Robichaud, P. Cicek, D. Deslandes, and F. Nabki, "Frequency Tuning Technique of Piezoelectric Ultrasonic Transducers for Ranging Applications," *Journal of Microelectromechanical Systems*, vol. 27, no. 3, pp. 570–579, Jun. 2018.

[7] X. Liu, X. Chen, X. Le, Z. Xu, C. Wu, and J. Xie, "A High-Performance Square pMUT for Range-finder," 2018, pp. 115–118.

[8] G.-H. Feng and H.-J. Liu, "Piezoelectric Micromachined Ultrasonic Transducers with a Cost-Effective Bottom-Up Fabrication Scheme for Millimeter-Scale Range Finding," *Sensors*, vol. 19, no. 21, p. 4696, Jan. 2019, number: 21 Publisher: Multidisciplinary Digital Publishing Institute. [Online]. Available: https://www.mdpi.com/1424-8220/19/21/4696

[9] H.-Y. Tang, Y. Lu, X. Jiang, E. J. Ng, J. M. Tsai, D. A. Horsley, and B. E. Boser, "3-D Ultrasonic Fingerprint Sensor-on-a-Chip," *IEEE Journal of Solid-State Circuits*, vol. 51, no. 11, pp. 2522–2533, Nov. 2016.

[10] R. J. Przybyla, H.-Y. Tang, S. E. Shelton, D. A. Horsley, and B. E. Boser, "12.1 3D ultrasonic gesture recognition," in *2014 IEEE International Solid-State Circuits Conference Digest of Technical Papers (ISSCC)*, Feb. 2014, pp. 210–211, iSSN: 2376-8606.

[11] F. Amirkhan, A. Robichaud, X. Ropagnol, M. Gratuze, T. Ozaki, F. Nabki, and F. Blanchard, "Active terahertz time differentiator using piezoelectric micromachined ultrasonic transducer array," *Optics Letters*, vol. 45, no. 13, pp. 3589–3592, Jul. 2020. [Online]. Available: https://www.osapublishing.org/ol/abstract.cfm?uri=ol-45-13-3589

[12] F. Amirkhan, M. Gratuze, X. Ropagnol, O. Tsuneyuki, F. Nabki, and F. Blanchard, "Terahertz time-domain derivative spectrometer using a large-aperture piezoelectric micromachined device," *Optics Express*, 2021. [Online]. Available: Optics Express

[13] F. Amirkhan, A. Robichaud, X. Ropagnol, M. Gratuze, T. Ozaki, F. Nabki, and F. Blanchard, "Simulation study of a piezoelectric micromachined ultrasonic transducer as terahertz differentiator," in *OSA Advanced Photonics Congress (AP) 2020 (IPR, NP, NOMA, Networks, PVLED, PSC, SPPCom, SOF) (2020), paper NoM4C.5*. Optical Society of America, Jul. 2020, p. NoM4C.5. [Online]. Available: https://www.osapublishing.org/abstract.cfm?uri=NOMA-2020-NoM4C.5

[14] A. Robichaud, D. Deslandes, P. Cicek, and F. Nabki, "A Novel Topology for Process Variation-Tolerant Piezoelectric Micromachined Ultrasonic Transducers," *Journal of Microelectromechanical Systems*, vol. 27, no. 6, pp. 1204–1212, Dec. 2018.

[15] X. Chen, D. Chen, X. Liu, D. Yang, J. Pang, and J. Xie, "Transmitting Sensitivity Enhancement of Piezoelectric Micromachined Ultrasonic Transducers via Residual Stress Localization by Stiffness Modification," *IEEE Electron Device Letters*, vol. 40, no. 5, pp. 796–799, May 2019.

[16] L. Wu, X. Chen, G. Wang, and Q. Zhou, "Dual-frequency piezoelectric micromachined ultrasonic transducers," *Applied Physics Letters*, vol. 115, no. 2, 2019.

[17] J. Liu, C. Oakley, and R. Shandas, "Capacitive micromachined ultrasonic transducers using commercial multi-user MUMPs process: Capability and limitations," *Ultrasonics*, vol. 49, no. 8, pp. 765–773, Dec. 2009. [Online]. Available: http://www.sciencedirect.com/science/article/pii/S0041624X09000729

[18] L. Song, "Application of electroless plating for fabrication of flexible and integrated piezoelectric ultrasonic sensors," Ph.D. dissertation, McGill, 2008.

[19] H. Cho, B. Jeong, M.-F. Yu, A. F. Vakakis, D. M. McFarland, and L. A. Bergman, "Nonlinear hardening and softening resonances in micromechanical cantilever-nanotube systems originated from nanoscale geometric nonlinearities," *International Journal of Solids and Structures*, vol. 49, no. 15, pp. 2059–2065, Aug. 2012. [Online]. Available: http://www.sciencedirect.com/science/article/pii/S0020768312001631

[20] Y. Wei, Y. Dong, X. Huang, and Z. Zhang, "A Stepped Frequency Sweeping Method for Nonlinearity Measurement of Microresonators," *Sensors*, vol. 16, no. 10, p. 1700, Oct. 2016. [Online]. Available: https://www.mdpi.com/1424-8220/16/10/1700

[21] S. Nabavi and L. Zhang, "Nonlinear Multi-mode Wideband Piezoelectric MEMS Vibration Energy Harvester," *IEEE Sensors Journal*, pp. 1–1, 2019.

[22] C. Comi, A. Corigliano, V. Zega, and S. Zerbini, "Non linear response and optimization of a new z-axis resonant micro-accelerometer," *Mechatronics*, vol. 40, pp. 235–243, Dec. 2016. [Online]. Available: http://www.sciencedirect.com/science/article/pii/S0957415816300514

[23] X. Zou and A. Seshia, "Non-Linear Frequency Noise Modulation in a Resonant MEMS Accelerometer," *IEEE Sensors Journal*, vol. 17, no. 13, pp. 4122–4127, 2017.

[24] A. Frangi, A. Guerrieri, N. Boni, R. Carminati, M. Soldo, and G. Mendicino, "Mode Coupling and Parametric Resonance in Electrostatically Actuated Micromirrors," *IEEE Transactions on Industrial Electronics*, vol. 65, no. 7, pp. 5962–5969, Jul. 2018.

[25] S. Tiwari and R. N. Candler, "Using flexural MEMS to study and exploit nonlinearities: a review," *Journal of Micromechanics and Microengineering*, vol. 29, no. 8, p. 083002, Jun. 2019.

[26] Y. Jia, S. Du, and A. A. Seshia, "Twenty-Eight Orders of Parametric Resonance in a Microelectromechanical Device for Multi-band Vibration Energy Harvesting," *Scientific Reports*, vol. 6, p. 30167, Jul. 2016. [Online]. Available: https://www.nature.com/articles/srep30167

[27] M. Rezaeisaray, M. E. Gowini, D. Sameoto, D. Raboud, and W. Moussa, "Low frequency piezoelectric energy harvesting at multi vibration mode shapes," *Sensors and Actuators A: Physical*, vol. 228, pp. 104–111, Jun. 2015. [Online]. Available: http://www.sciencedirect.com/science/article/pii/S0924424715001004

[28] M. Defoort, L. Rufer, and S. Basrour, "Chaotic ultrasound generation using a nonlinear piezoelectric microtransducer," *Journal of Micromechanics and Microengineering*, vol. 31, no. 5, p. 054002, Apr. 2021. [Online]. Available: https://iopscience.iop.org/article/10.1088/1361-6439/abf365/meta

[29] D. Chen, Y. Wang, Y. Guan, X. Chen, X. Liu, and J. Xie, "Methods for Nonlinearities Reduction in Micromechanical Beams Resonators," *Journal of Microelectromechanical Systems*, vol. 27, no. 5, pp. 764–773, Oct. 2018.

[30] Chengqun Gui, R. Legtenberg, H. Tilmans, J. Fluitman, and M. Elwenspoek, "Nonlinearity and hysteresis of resonant strain gauges," *Journal of Microelectromechanical Systems*, vol. 7, no. 1, pp. 122–127, Mar. 1998.

[31] H. M. Ouakad and M. I. Younis, "The dynamic behavior of MEMS arch resonators actuated electrically," *International Journal of Non-Linear Mechanics*, vol. 45, no. 7, pp. 704–713, Sep. 2010. [Online]. Available: http://www.sciencedirect.com/science/article/pii/S0020746210000594

[32] J. Zhao, S. Zhou, B. Wang, and X. Wang, "Nonlinear microbeam model based on strain gradient theory," *Applied Mathematical Modelling*, vol. 36, no. 6, pp. 2674–2686, Jun. 2012. [Online]. Available: https://www.sciencedirect.com/science/article/pii/S0307904X1100607X

[33] B. Sajadi, F. Alijani, H. Goosen, and F. van Keulen, "Effect of pressure on nonlinear dynamics and instability of electrically actuated circular micro-plates," *Nonlinear Dynamics*, vol. 91, no. 4, pp. 2157–2170, Mar. 2018. [Online]. Available: https://doi.org/10.1007/s11071-017-4007-y

[34] V. Zega, G. Langfelder, L. G. Falorni, and C. Comi, "Hardening, Softening, and Linear Behavior of Elastic Beams in MEMS: An Analytical Approach," *Journal of Microelectromechanical Systems*, vol. 28, no. 2, pp. 189–198, Apr. 2019.

[35] N. Alcheikh, H. M. Ouakad, and M. I. Younis, "Dynamic analysis of straight stepped microbeams," *International Journal of Non-Linear Mechanics*, vol. 128, p. 103639, Jan. 2021. [Online]. Available: https://www.sciencedirect.com/science/article/pii/S0020746220303012

[36] M. J. Brennan, I. Kovacic, A. Carrella, and T. P. Waters, "On the jump-up and jump-down frequencies of the Duffing oscillator," *Journal of Sound and Vibration*, vol. 318, no. 4, pp. 1250–1261, Dec. 2008. [Online]. Available: http://www.sciencedirect.com/science/article/pii/S0022460X08003805

[37] I. Kovacic and M. J. Brennan, *The Duffing Equation: Nonlinear Oscillators and their Behaviour*, 1st ed. John Wiley and Sons, 2011. [Online]. Available: https://www.wiley.com/en-ca/The+Duffing+Equation:+Nonlinear+Oscillators+and+their+Behaviour-p-9780470715499

[38] M. Gratuze, A.-H. Alameh, S. Nabavi, and F. Nabki, "Control of Spring Softening and Hardening in the Squared Daisy," *Micromachines*, vol. 12, no. 4, p. 448, Apr. 2021. [Online]. Available: https://www.mdpi.com/2072-666X/12/4/448

[39] M. Gratuze, A. H. Alameh, and F. Nabki, "Design of the Squared Daisy: A Multi-Mode Energy Harvester, with Reduced Variability and a Non-Linear Frequency Response," *Sensors*, vol. 19, no. 15, p. 3247, Jan. 2019. [Online]. Available: https://www.mdpi.com/1424-8220/19/15/3247

[40] A. H. Alameh, M. Gratuze, and F. Nabki, "Impact of Geometry on the Performance of Cantilever-based Piezoelectric Vibration Energy Harvesters," *IEEE Sensors Journal*, pp. 1–1, 2019.

[41] J. Pons-Nin, S. Gorreta, M. Dominguez, E. Blokhina, D. O'Connell, and O. Feely, "Design and test of resonators using PiezoMUMPS technology," in *2014 Symposium on Design, Test, Integration and Packaging of MEMS/MOEMS (DTIP)*, Apr. 2014, pp. 1–6.

[42] A. H. Alameh, M. Gratuze, M. Y. Elsayed, and F. Nabki, "Effects of Proof Mass Geometry on Piezoelectric Vibration Energy Harvesters," *Sensors*, vol. 18, no. 5, p. 1584, May 2018. [Online]. Available: https://www.mdpi.com/1424-8220/18/5/1584

[43] A. Cowen, G. Hames, K. Glukh, and B. Hardy, *PiezoMUMPs design handbook*. MEMSCAP Inc, 2014.

[44] A. Nastro, L. Rufer, M. Ferrari, S. Basrour, and V. Ferrari, "Piezoelectric Micromachined Acoustic Transducer with Electrically-Tunable Resonant Frequency," in *2019 20th International Conference on Solid-State Sensors, Actuators and Microsystems Eurosensors XXXIII (TRANSDUCERS EUROSENSORS XXXIII)*, Jun. 2019, pp. 1905–1908, iSSN: 2167-0021.

[45] R. O. Guldiken, M. Balantekin, J. Zahorian, and F. L. Degertekin, "Characterization of dual-electrode CMUTs: demonstration of improved receive performance and pulse echo operation with dynamic membrane shaping," *IEEE Transactions on Ultrasonics, Ferroelectrics, and Frequency Control*, vol. 55, no. 10, pp. 2336–2344, Oct. 2008.

[46] A. Robichaud, D. Deslandes, P.-V. Cicek, and F. Nabki, "Electromechanical Tuning of Piecewise Stiffness and Damping for Long-Range and High-Precision Piezoelectric Ultrasonic Transducers," *Journal of Microelectromechanical Systems*, pp. 1–10, 2020.

[47] X. Liu, X. Chen, X. Le, Y. Wang, C. Wu, and J. Xie, "Reducing ring-down time of pMUTs with phase shift of driving waveform," *Sensors and Actuators A: Physical*, vol. 281, pp. 100–107, Oct. 2018. [Online]. Available: https://www.sciencedirect.com/science/article/pii/S0924424718306083

[48] Z. Wu, W. Liu, Z. Tong, S. Zhang, Y. Gu, G. Wu, A. Tovstopyat, C. Sun, and L. Lou, "A Novel Transfer Function Based Ring-Down Suppression System for PMUTs," *Sensors*, vol. 21, no. 19, p. 6414, Jan. 2021. [Online]. Available: https://www.mdpi.com/1424-8220/21/19/6414

[49] F. V. Pop, B. Herrera, C. Cassella, and M. Rinaldi, "Direct Modulation Piezoelectric Micro-Machined Ultrasonic Transducer System (DMUT)," in *2019 IEEE 32nd International Conference on Micro Electro Mechanical Systems (MEMS)*, Jan. 2019, pp. 61–64, iSSN: 2160-1968.

[50] F. Pop, B. Herrera, C. Cassella, and M. Rinaldi, "Modeling and Optimization of Directly Modulated Piezoelectric Micromachined Ultrasonic Transducers," *Sensors*, vol. 21, no. 1, p. 157, Jan. 2021. [Online]. Available: https://www.mdpi.com/1424-8220/21/1/157

Mathieu Gratuze (S'19) received a Master's Degree with a major in electronics and microelectronics architecture from the École Supérieure de Chimie Physique Électronique de Lyon (CPE Lyon), Lyon, France, in 2017, and a M.Sc. degree in electrical and electronic engineering from École Centrale de Lyon (Centrale Lyon), France, in 2017. He is currently pursuing a Ph.D. degree with the LaCIME (Laboratoire de Communications et d'Intégration de la MicroÉlectronique), Department of Electrical Engineering, in the École de Technologie Supérieure, Montréal, Qc, Canada. His research interests include design, modeling and characterization of piezoelectric MEMS transducers for energy harvesting and sensor applications.

Abdul-Hafiz Alameh (S'15-M'19) received the M.A.Sc. degree in electrical engineering from Université du Québec á Montréal (UQAM), Montréal, QC, Canada, in 2015, and the Ph.D. degree in electrical engineering from École de Technologie Supérieure (ÉTS), Université du Québec, Montréal, QC, Canada in 2019. He was with the Communications and Microelectronic Integration Laboratory (LACIME) and he is currently with Spark Microsystems, Montreal, QC, Canada. His research interests include power management and energy harvesting applications, MEMS interface circuits and MEMS transducers.

Dr. Alameh has held scholarships from the Microsystems Strategic Alliance of Quebec (ReSMiQ) and the Quebec Fund for Research in Nature and Technology (FRQNT)

Alexandre Robichaud (M) received the B.Eng. degree (Hons.) in microelectronics engineering from the Université du Québec à Montréal, Canada, in 2013, the M.Eng. degree (Hons.) in electrical engineering and the Ph.D. degree (Hons.) in electrical engineering from the École de technologie supérieure, Monntreal, QC, Canada, in 2015 and 2020 respectively. He has held scholarship from the Natural Sciences and Engineering Research Council of Canada (NSERC) and the Quebec Fund for Research in Nature and Technology (FQRNT). His research interests include MEMS design and fabrication, electronic design, and ultrasound imaging.

In 2019, he joined the "Université du Québec à Chicoutimi" (UQAC), Chicoutimi, QC, Canada, where he is a Professor in Electrical Engineering.

Frederic Nabki (S'99–M'10) received the B.Eng. degree in electrical engineering with honors and the Ph.D. degree in electrical engineering from McGill University, Montreal, QC, Canada, in 2003 and 2010, respectively.

In 2008, he joined the "Université du Québec à Montréal" (UQAM), Montreal, QC, Canada, where he was an Associate Professor in Microelectronics Engineering. In 2016, he joined the "École de Technologie Supérieure", Montreal, QC, Canada, a constituent of the University of Quebec, as an Associate Professor in the Department of Electrical Engineering, where he is since 2019 a Full Professor. His research interests include microelectromechanical systems (MEMS) and RF/analog microelectronics, specifically focusing on the creation of next-generation MEMS processes using advanced materials, the integration of MEMS devices with CMOS systems, the modeling of MEMS devices, and the design of CMOS phase-locked loops, ultra-wideband transceivers, and MEMS interface circuits. He has published two book chapters, edited one book and co-authored over 120 publications. He holds 32 issued patents related to MEMS and CMOS/MEMS monolithic integration.

Dr. Nabki is a member of the Quebec Order of Engineers. He served as the Secretary and Treasurer of the Montreal Section of the IEEE from 2013 to 2015 and 2015 to 2017, respectively. Professor Nabki jointly manages the Microtechnology and Microsystems Laboratory. He was a recipient of the Governor General of Canada's Academic Bronze Medal, the J.J. Archambault IEEE Canada Medal and the UQAM Faculty of Science Early Career Research Award. He holds or has held financial support from the Microsystems Strategic Alliance of Quebec (ReSMiQ), the Quebec Fund for Research in Nature and Technology (FRQNT), the Natural Sciences and Engineering Research Council of Canada (NSERC), and the Canada Foundation for Innovation (CFI).